Activity of the *C. elegans* egg-laying behavior circuit is controlled by competing activation and feedback inhibition

Kevin M. Collins[1,2,6], Addys Bode[1], Robert W. Fernandez[2], Jessica E. Tanis[2,4], Jacob Brewer[2], Matt Creamer[3,5], and Michael R. Koelle[2,3]

[1] Department of Biology, University of Miami, Coral Gables, FL USA

[2] Department of Molecular Biophysics and Biochemistry, Yale University, New Haven, CT USA

[3] Interdepartmental Neuroscience Program, Yale University, New Haven, CT USA

[4] Present address: Department of Biological Sciences, University of Delaware, Newark, DE USA

[5] Present address: Department of Molecular, Cellular, and Developmental Biology, Yale University, New Haven, CT USA

[6]To whom correspondence should be addressed:

kcollins@bio.miami.edu

Department of Biology

University of Miami

1301 Memorial Drive

Coral Gables, FL 33143

Tel: (305) 284-9058

Abstract

Like many behaviors, *Caenorhabditis elegans* egg laying alternates between inactive and active states. To understand how the underlying neural circuit turns the behavior on and off, we optically recorded circuit activity in behaving animals while manipulating circuit function using mutations, optogenetics, and drugs. In the active state, the circuit shows rhythmic activity phased with the body bends of locomotion. The serotonergic HSN command neurons initiate the active state, but accumulation of unlaid eggs also promotes the active state independent of the HSNs. The cholinergic VC motor neurons slow locomotion during egg-laying muscle contraction and egg release. The uv1 neuroendocrine cells mechanically sense passage of eggs through the vulva and release tyramine to inhibit egg laying, in part via the LGC-55 tyramine-gated Cl^- channel on the HSNs. Our results identify discrete signals that entrain or detach the circuit from the locomotion central pattern generator to produce active and inactive states.

35 **Introduction**

36 Neural circuits are the functional units underlying all thoughts and behaviors, but there is
37 as yet no neural circuit in any organism for which we know with precision how the many
38 signaling events among its cells together generate its activity. This would require, among other
39 things, understanding how neuromodulators shape activity at chemical and electrical synapses
40 to alter the excitability of specific cells in the circuit to generate regulated, dynamic patterns of
41 circuit responses and a coherent behavioral output. One approach to this problem is to analyze
42 small neural circuits typical of invertebrate model organisms, so that both the simplicity of the
43 circuits and the powerful experimental approaches uniquely possible within these systems can
44 provide a penetrating analysis (Marder, 2012).

45 *C. elegans* egg-laying behavior is controlled by a small circuit that offers many
46 experimental advantages for study (Schafer, 2006). This circuit, diagrammed in Figure 1A,
47 consists of two serotonergic Hermaphrodite Specific Neurons (HSNs) and six cholinergic
48 Ventral C neurons (VCs), each of which synapse onto a set of vulval muscles whose
49 contraction expels eggs. Four neuroendocrine uv1 cells also regulate egg laying (Jose et al.,
50 2007). Despite its anatomical simplicity, the egg-laying circuit produces a regulated, rhythmic
51 behavior that alternates between quiescent periods of about 20 minutes during which no egg
52 laying occurs, and active states lasting a few minutes during which ~5 eggs are laid
53 (Waggoner et al., 1998). Active states appear to result when the HSNs release serotonin that
54 signals through G protein coupled receptors on the vulval muscles to increase their excitability
55 (Waggoner et al., 1998; Shyn et al., 2003; Hapiak et al., 2009; Emtage et al., 2012). Strong
56 regulation by sensory stimuli is superimposed on the pattern of alternating behavioral states.
57 For example, carbon dioxide regulates neuropeptide release from head sensory neurons that

58 signal through receptors on the HSNs to inhibit egg laying (Ringstad and Horvitz, 2008; Hallem
59 et al., 2011). Worms also halt egg laying in the absence of food and restart the behavior when
60 re-fed (Daniels et al., 2000; Dong et al., 2000).

61 *C. elegans* egg laying has been studied for decades, and dozens of genes have been
62 identified by mutations that either reduce (Desai et al., 1988) or increase (Bany et al., 2003)
63 egg laying. Some of the identified genes encode ion channels that regulate cell and synaptic
64 electrical excitability (Elkes et al., 1997; Johnstone et al., 1997; Lee et al., 1997; Weinshenker
65 et al., 1999; Jospin et al., 2002; Jose et al., 2007; Collins and Koelle, 2013). Other identified
66 genes encode components of G protein signaling pathways that act in specific cells of the
67 circuit (Brundage et al., 1996; Koelle and Horvitz, 1996; Hajdu-Cronin et al., 1999; Miller et al.,
68 1999; Williams et al., 2007; Porter et al., 2010). These results suggest neuromodulators,
69 including serotonin, signal through G proteins to regulate the excitability of specific cells in the
70 circuit to control circuit activity and egg laying.

71 The ability to leverage egg-laying mutants to understand the molecular mechanisms that
72 initiate, sustain, and terminate the active state of egg laying has been limited by the tools
73 available to analyze activity in the cells of the egg-laying circuit. Ca^{2+} activity in cells in the
74 circuit was initially optically recorded in immobilized animals, which have limited ability to
75 engage in egg-laying behavior (Shyn et al., 2003; Zhang et al., 2008). More recently we
76 developed methods to optically record Ca^{2+} activity of the vulval muscles in moving animals as
77 they engage in normal egg-laying behavior. Using ratiometric imaging to correct for movement
78 and focus artifacts, and recording at 20 frames/sec for periods of up to one hour, we were able
79 to measure activity of the vulval muscles as animals cycled through active and inactive states
80 (Collins and Koelle, 2013; Li et al., 2013). Our recordings showed that the vulval muscles are

excited rhythmically in phase with the body bends of animal locomotion, and we proposed this was due to signaling from the cholinergic motor neurons, including the VCs, that are rhythmically active during locomotion. We found that a conserved ERG K^+ channel depresses response of the vulval muscles to excitation, thus maintaining the inactive behavior state, and we proposed that serotonin signaling onto vulval muscle receptors enhances vulval muscle excitability to allow the strong muscle contractions and egg release seen in the active state. We have now generated tools to carry out Ca^{2+} recordings in moving animals for each neuron type in the egg-laying circuit. Combining these recordings with precise manipulations of the circuit using mutations, optogenetics, and drugs allows us to deduce how specific signals from these cells drive specific features of circuit activity and behavior.

Results

Distinct patterns of activity in the egg-laying circuit accompany the active and inactive behavior states

We carried out long-term Ca^{2+} recordings of HSN and VC neuron activity in behaving animals using methods we developed previously for the vulval muscles (Collins and Koelle, 2013). We generated transgenic strains of *C. elegans* co-expressing the fluorescent Ca^{2+} reporter GCaMP5 and the Ca^{2+}-independent fluorescent protein mCherry specifically in the HSN or VC neurons, and used ratiometric imaging to record cell activity and egg-laying behavior as animals moved through active and inactive egg-laying states (Figure 1). Because of the large size of the egg-laying synapse, we were able to clearly observe Ca^{2+} transients localized to the presynaptic terminus in HSN (Figure 1B; Movie 1) and VC (Figure 1C; Movie 2).

103 For comparison, we also carried out Ca^{2+} recordings of vulval muscles, and as in our earlier
104 studies of these muscles, were able to clearly distinguish the weak twitching contractions
105 (Figure 1D; Movie 3) from the strong contractions that drove egg release (Figure 1E).

106 Through long-term Ca^{2+} imaging, we observed a striking increase in rhythmic activity in
107 the cells of the circuit that began prior to the first egg-laying event and persisted beyond the
108 last egg-laying event of each active state (Figure 1F). We defined the active state as one
109 minute before the first egg-laying event and one minute after the last egg-laying event.

110 We found that HSNs displayed long (~4 seconds at half-maximum amplitude) Ca^{2+}
111 transients that were largely consistent in waveform and amplitude, but that varied in occurring
112 either as single events or trains (Figure 1F). There was also significant HSN activity outside of
113 the active state, but HSN transients were more frequent during the active state (Figure 1G).
114 Active state HSN transients typically occurred in bursts, within which HSN transients occurred
115 every ~20 seconds (Figure 1G). Only 11% of HSN transients were accompanied by an egg
116 release (Figure 1H), but almost every egg-laying event occurred during an HSN transient
117 (Figure 1F; out of 49 total egg-laying events observed, 48 occurred within an HSN transient).

118 VC transients were shorter than HSN transients (~2 seconds at half-max) and variable
119 in amplitude. We rarely observed VC transients during the inactive state, but we found a clear
120 induction of transients during the active state (Movie 2; Figure 1F, G), and these transients
121 occurred in bursts around egg-laying events with an inter-transient interval of ~10 seconds,
122 about twice as frequent as seen for the HSNs. Although Ca^{2+} transients were most intense in
123 the VC presynaptic varicosities and axonal processes, they were also visible in all six VC cell
124 bodies, especially those of the VC4 and VC5 neurons that most closely flank the vulva (Figure
125 1C and Movie 2). Vulval muscle twitching and egg-laying contractions caused significant

126 mechanical deformation of the VC neurons. 34% of VC transients were accompanied by an
127 egg release, a larger fraction than seen for HSN and vulval muscle Ca^{2+} transients (Figure 3H,
128 p <0.0001; Fisher's exact test). Every egg-release event was accompanied by a VC transient.
129 There was no correlation seen between the magnitudes of VC or HSN transients that did or did
130 not coincide with egg release, while the magnitude of muscle Ca^{2+} transients that resulted in
131 egg laying were ~4-fold larger than the muscle twitch transients that did not release eggs
132 (Figure 1H).

133 The close apposition of HSN, VC, and vulval muscle synaptic regions prevented us from
134 simultaneously imaging more than one cell type, but we were able to compare timing of activity
135 in the different cells using the moment of egg release as an objective landmark. HSN Ca^{2+}
136 transients peaked ~2 seconds prior to egg release (Figure 1I) and decayed slowly. Shorter VC
137 Ca^{2+} transients followed HSN activity, peaking ~0.1 seconds before egg release. Vulval muscle
138 Ca^{2+} transients peaked with egg laying. We also tracked vulval muscle contraction by
139 measuring the size and fluorescence intensity of the mCherry labeled muscles, and saw that
140 muscle relaxation and decay of vulval muscle Ca^{2+} immediately followed egg release (Figure
141 1I).

142

143 **HSN, VC, and vulval muscle activity are phased with animal locomotion**

144 *C. elegans* moves with sinusoidal body bends consisting of waves of body-wall muscle
145 contraction driven by the Ventral A and B (VA/VB) ventral nerve cord motor neurons. We
146 previously observed that vulval muscle Ca^{2+} transients occurred rhythmically when the vulva
147 was at a particular phase of the locomotion body bend (Collins and Koelle, 2013). Using our

148 video recordings of Ca^{2+} activity in moving animals, we examined whether HSN and VC activity
149 are similarly phased with locomotion. Thus we determined timing of the peaks of HSN, VC, and
150 vulval muscle Ca^{2+} transients relative to when the vulva passed through the previous and
151 subsequent most contracted or relaxed state of a body bend. The results were plotted on
152 circular histograms with ventral contraction at 0/360°, ventral relaxation at 180°, and
153 intermediate phases of body bends at the angles in between (Figure 2A). We found that the
154 HSN, VC, and vulval muscle Ca^{2+} transients occurred when the vulva was at particular phases
155 of the locomotor body bend. HSN transients just prior to egg release reached their maximum at
156 ~180°, when the vulva and adjacent body wall muscles were at their most relaxed state (Figure
157 2B). VC and vulval muscle transients that accompanied egg laying occurred later, starting at
158 ~225° and 270°, respectively (Figure 2C and 2D). HSN transients that did not result in egg
159 laying showed no clear evidence of phasing (Figure 2B). In contrast, VC transients and vulval
160 muscle twitch transients that did not lead to egg release were still phased, but delayed by ~45°
161 toward the most ventral contracted state. These results confirm our previous observations that
162 vulval muscle twitching and egg-laying activity are phased with locomotion (Collins and Koelle,
163 2013). These results extend that analysis to show that HSN, VC, and vulval muscle activity
164 during egg laying events occur earlier in the body bend cycle, when the adjacent body wall
165 muscles are in a more relaxed state.

166

167 **Optogenetic activation of HSNs initiates the egg-laying active state**

168 To directly test how neurotransmitter signaling from the HSNs regulates egg-laying
169 circuit activity, we used the *egl-6* promoter to express Channelrhodopsin-2 in the HSNs
170 (Emtage et al., 2012), allowing us to drive neurotransmitter release specifically from the HSNs

171 with blue light. We repeated the observation of Emtage et al. (2012) that optogenetic activation
172 of HSNs stimulates egg-laying behavior (Movie 4), but we activated the HSNs while
173 simultaneously recording behavior and Ca^{2+} activity in the VCs (Figure 3A) or vulval muscles
174 (Figure 3B). We found that activation of HSNs resulted in circuit activity reminiscent of a
175 spontaneous active state, including rhythmic Ca^{2+} activity of both VCs and vulval muscles, and
176 egg-laying events that accompanied a subset of these Ca^{2+} transients. Some differences from
177 a spontaneous active state were notable. Almost every VC transient after optogenetic HSN
178 activation was accompanied by an egg-laying event, whereas only one third of VC transients
179 during spontaneous active states were accompanied by egg-laying events. These results
180 suggest that the high level of HSN activity after optogenetic activation induces strong coupling
181 of VC and vulval muscle excitation.

182 During both spontaneous and optogenetically-induced active states, rhythmic vulval
183 muscle twitches occur far more frequently than do VC transients, suggesting these twitches
184 are excited by something other than the VCs. Careful observation shows that the most
185 dramatic Ca^{2+} changes during vulval muscle twitching occur at the ventral tips of the vm1
186 muscles (Figure 1D). The VCs innervate vm2 muscles but not the vm1 muscles. The vm1
187 muscles are instead innervated by the VB6 and VA7 neurons that also release acetylcholine to
188 drive body wall muscle contraction for locomotion (White, J.G. et al., 1986). Consistent with
189 this, vm1 twitching occurs at the same time the adjacent ventral body wall muscles are
190 contracting during locomotion (Figure 2D). Increased electrical excitability of the vulval muscles
191 during a spontaneous or optogenetically-induced active state may allow for vm1 excitation by
192 VB6/VA7 with each body bend.

193

194 **VC neuron activity helps coordinate egg laying and locomotion**

195 Our observation that VC activity always accompanies egg release (Figure 1I and 3A) is
196 consistent with a proposal that the VCs release acetylcholine that signals through vulval muscle
197 nicotinic receptors to drive egg laying (Waggoner et al., 2000; Kim et al., 2001). While VC4 and VC5
198 make extensive synapses onto the vm2 muscles, VC1-3 and VC6 make extensive, distributed
199 synapses onto the ventral body wall muscles (White et al., 1976). How VC activity during egg
200 laying might affect body wall muscle contraction has not been examined. We optogenetically
201 activated the HSNs to induce active states and recorded animal speed around egg-laying
202 events (Figure 3C). We found a clear and significant reduction of locomotion speed beginning
203 ~1 s before egg release, a time when VC activity is increasing (Figure 1I). Locomotion speed
204 recovered immediately after egg release (Figure 3C). These results are consistent with the
205 hypothesis that acetylcholine released from the VCs slows locomotion during egg laying.

206 To test directly how VC activity regulates locomotion and egg laying, we used a *lin-11*
207 promoter fragment to express Channelrhodopsin-2 specifically in the VCs (Bany et al., 2003).
208 Optogenetic activation of the VCs was not sufficient to drive egg laying (Figure 3F), but did
209 lead to a rapid shortening of the body (Movie 5 and Figure 3D) and cessation of locomotion
210 (Figure 3E). The shortening phenotype seen in VC ChR2 animals after blue light exposure
211 closely resembles that seen for optogenetic activation of the body wall muscles (Nagel et al.,
212 2005), except the head and tail of VC-activated animals were still mobile and active, consistent
213 with the fact that VC neurons innervate only the central body wall muscles (White et al., 1976).
214 Our results indicate that while VC activity immediately precedes egg-laying events, it is not
215 sufficient to drive egg release. Optogenetic VC activation is sufficient to produce a slowing of
216 locomotion as seen during egg-laying events. In contrast, HSN activity is sufficient to induce all

217 of the hallmarks of the active state, including rhythmic vulval muscle twitching, VC transients,
218 and the coordinated vulval muscle contractions that produce egg-laying events.

219

220 **Animals lacking HSNs still enter the egg-laying active state**

221 We next tested whether HSN activity was necessary for circuit activity by recording
222 vulval muscle activity in *egl-1(dm)* mutants, which lack HSN neurons (Trent et al., 1983).
223 Animals lacking HSNs have a substantial lengthening of the inactive state (Waggoner et al.,
224 1998) and are strongly egg-laying defective, accumulating ~50 eggs in the uterus rather than
225 the 12-15 seen in the wild type (Trent et al., 1983). We expected to find that loss of HSNs led
226 to a dramatic reduction in vulval muscle activity. Surprisingly, we found the opposite; animals
227 lacking HSNs had more frequent vulval muscle Ca^{2+} transients during the inactive state and
228 robust activity during infrequent active states that led to multiple eggs being laid in a short
229 period (compare Figures 4A and 4B; quantitation in Figure 4C). There was a significant
230 reduction in the amplitude of vulval muscle Ca^{2+} transients during egg laying in *egl-1(dm)*
231 mutants while the amplitude of twitch Ca^{2+} transients was unaffected (Fig. 4D). Vulval muscle
232 activity in *egl-1(dm)* mutants lacking HSNs resembled the frequent yet uncoordinated vulval
233 muscle activity found in animals missing the vm2 vulval muscle arms onto which the HSNs
234 normally make synapses (Li et al., 2013). Such activity involves asynchronous contraction of
235 the anterior and posterior vulval muscles, which is ineffective at allowing egg release. One
236 quantitative measure of this asynchrony is that overall vulval muscle Ca^{2+} transient peaks in
237 *egl-1(dm)* mutants were longer in duration, likely resulting in individual muscle cells beginning
238 their transients at different times (Figure 4E). Vulval muscle Ca^{2+} transients in animals lacking
239 HSNs remained phased with locomotion, including the ~45° advance in phase of vulval muscle

240 activity that results in egg-laying events (compare Figures 4F and 4G). These results suggest
241 that the HSNs are necessary to coordinate contraction of anterior and posterior vulval muscles,
242 and that signals from other cells besides the HSNs can also induce the egg-laying active state.

243 We hypothesized that accumulating unlaid eggs could stretch the uterus or body,
244 leading to signals responsible for the increased activity of the vulval muscles independent of
245 neurotransmitter signaling from the HSNs. To test if egg accumulation contributed to the onset
246 of the active phase, we sterilized animals with FUDR (Mitchell et al., 1979), a DNA synthesis
247 inhibitor that blocks germ line cell division and thus egg production. FUDR-treated animals had
248 a dramatic reduction of vulval muscle activity and appeared to be stuck in the inactive state,
249 with no egg-laying transients observed (Figures 4A and 4B). The inhibition of vulval muscle
250 activity by FUDR occurred in both wild-type animals and HSN-deficient *egl-1(dm)* mutants
251 (Figures 4C and 4D). The residual vulval muscle Ca^{2+} twitch transients in FUDR-treated
252 animals had phasing identical to those seen in the inactive state of untreated animals (Figures
253 4F and 4G). These results suggest that germ line activity and/or the accumulation of eggs in
254 the uterus is required to initiate the egg-laying active state.

255

256 **The uv1 neuroendocrine cells are mechanically deformed and activated by egg-laying**
257 **events**

258 We previously identified a role for the uv1 neuroendocrine cells in inhibiting egg-laying
259 behavior (Jose et al., 2007). The four uv1 cells sit at the junction between the uterine lumen
260 and the vulval canal (Newman and Sternberg, 1996), and as such are positioned to
261 mechanically sense the accumulation of unlaid eggs in the uterus and/or passage of eggs

262 through the vulval canal as they are laid. To record uv1 Ca^{2+} activity, we co-expressed
263 GCaMP5 and mCherry in uv1 from the *ocr-2* promoter and made recordings in behaving
264 animals. We found that the uv1 cells were mechanically deformed as each egg passed through
265 the vulva, and then showed strong Ca^{2+} transients after egg release (Figure 5A-B; Movie 5).
266 Egg-laying events did not always trigger Ca^{2+} transients in uv1, with uv1-silent events usually
267 being the first or last within an active state (data not shown). We also observed weaker uv1
268 Ca^{2+} transients a few minutes before or after the egg-laying active state (Figure 5B-D).
269 Because these were not closely associated with egg-laying events their functional importance
270 remains unclear. Typical active state uv1 Ca^{2+} transients began immediately with or slightly
271 before egg release, coinciding with the initial mechanical deformation of uv1 caused by the egg,
272 with the Ca^{2+} transient peak occurring ~2 seconds later (Figure 5E). Based on the position of
273 the uv1 cells, their morphological deformations during passage of eggs, and the timing of uv1
274 Ca^{2+} transients, our data suggest the uv1 cells are mechanically activated by eggs passing
275 through the vulva during egg laying.

276

277 **Tyramine signals through LGC-55 receptors to inhibit HSN activity and egg laying**

278 The uv1 cells make the biogenic amine neurotransmitter tyramine, and *tdc-1* mutations
279 that disrupt tyramine biosynthesis lead to increased egg-laying behaviors (Alkema et al., 2005).
280 We found that exogenous tyramine reduced egg laying in wild-type animals (Figure 6A). To
281 identify targets of tyramine inhibition, we tested response to exogenous tyramine in strains
282 mutant for three known *C. elegans* tyramine receptors. Animals lacking *lgc-55*, which encodes
283 a tyramine-gated Cl^- channel, showed resistance to inhibition by exogenous tyramine (Figure
284 6A), although tyramine at high levels still had a residual ability to reduce egg laying in *lgc-55*

285 mutants (Figure 6B). We transformed into *C. elegans* a fosmid transgene containing the full-
286 length *lgc-55* gene fused to GFP coding sequences, and found LGC-55 is expressed in the
287 HSNs, uv1, and vulval muscles (Figure 6C and Pirri et al., 2009). Re-expression of LGC-55
288 specifically in HSN from the *tph-1* promoter restored tyramine sensitivity to *lgc-55* mutants
289 (Figure 6D). We have previously shown that two Cl^- extruding transporters, KCC-2 and ABTS-1,
290 are expressed in the HSNs where they promote the development of inhibitory ligand-gated Cl^-
291 channel signaling (Tanis et al., 2009; Bellemer et al., 2011). These data suggest that tyramine
292 signaling through LGC-55 would hyperpolarize the HSN and inhibit activity. To test this directly,
293 we compared HSN activity in wild-type and *lgc-55* mutant animals. We observed a significant
294 increase in the frequency of Ca^{2+} transients in HSNs of *lgc-55* mutant animals (Figures 6E and
295 6F) in both the inactive and active states of egg-laying behavior. Mean HSN inter-transient
296 intervals in wild-type animals were 41±5 seconds in the inactive state and 17±2 seconds during
297 the active state, while intervals in *lgc-55* mutants were reduced to 22±2 seconds in the inactive
298 state and 13±1 seconds during the active state. Thus, the absence of inhibitory feedback by
299 tyramine signaling onto the HSNs leads to increased activity in both the active and inactive
300 egg-laying behavior states.

301

302 **Discussion**

303 Using a combination of optogenetic, molecular genetic, and Ca^{2+} imaging approaches,
304 we show an unexpected level of coordination of *C. elegans* egg-laying circuit activity by the
305 rhythm of locomotion and by egg production. Using recordings of cell activity in behaving
306 animals as they transition from the inactive to active egg-laying states, we were able to show
307 that circuit activity is diminished during the inactive state, strongly increased and rhythmic

308 during the active state, and this rhythm is phased with sinusoidal locomotion. Sterilization
309 eliminated the active state rhythm, locking animals in the inactive state. Our results suggest
310 that activity in the egg-laying circuit, like that of many other modulated motor circuits, responds
311 to rhythmic input from central pattern generators (Marder et al., 2015).

312 A working model shown in Figure 7 explains how different inputs into the egg-laying
313 circuit are responsible for the inactive state and the active state rhythms observed during egg-
314 laying behavior. Active state vulval muscle Ca^{2+} transients peak rhythmically each time the
315 vulva approaches a ventral body bend, the point at which the cholinergic VB and VA motor
316 neurons release acetylcholine to rhythmically excite both the vm1 muscles and adjacent
317 ventral body wall muscles during locomotion. During the inactive state, K^+ channels including
318 ERG depress vulval muscle excitability below threshold, explaining why we fail to observe
319 vulval muscle activity with each body bend during this state (Collins and Koelle, 2013). While
320 we observe rhythmic activity in the HSNs in the active phase, the periodicity and phasing of
321 HSN activity does not correlate with that of locomotion. Consistent with this, previous work
322 found changes in osmolarity can drive rhythmic HSN activity even in immobilized animals
323 (Zhang et al., 2008). Thus HSN rhythmic activity is independent of locomotion, although we
324 found HSN Ca^{2+} transients that happen to fall at a specific phase of locomotor body bends are
325 more likely to be followed by egg release. We propose that release of serotonin from the HSNs,
326 along with an unknown signal resulting from mechanical stretch of the uterus by accumulating
327 eggs, together raise vulval muscle electrical excitability to result in the active state during which
328 the vulval muscles undergo rhythmic twitching or egg laying contractions in response to the
329 same cholinergic VA and VB neurons that drive locomotor body bends. This model accounts
330 for the phasing of vm1 transients with body bends, although egg-laying events require

331 additional activity in the vm2 muscles that results in the coordinated contraction of all vm
332 muscles that results in egg release. We found that vm transients that lead to egg release are
333 on average slightly phase advanced relative to those that do not. This phase advance could
334 from the excitatory input onto the vm2 muscles occurring earlier in the body bend, and
335 candidates for this input are the HSNs and VCs, both of which synapse onto the vm2 muscles
336 and have phased activity during egg-laying events. The functional purpose of this phase
337 advance may be mechanical. Passage of each 25x40μm egg requires contraction of vm1 and
338 vm2 muscles on both the anterior and posterior sides of the vulva (Li et al., 2013). There may
339 not be sufficient room for vulva to fully open and release egg unless the adjacent body wall
340 muscles are in a contracted state.

341 The HSNs are command neurons that integrate diverse sensory inputs and initiate the
342 ~2 minute active state of the egg-laying circuit. Optogenetic activation of HSNs recapitulates
343 features of the active state including phased VC and vulval muscle activity and multiple egg-
344 laying events. However, stimulation of the HSNs fails to drive tetanic contraction of the vulval
345 muscles as would be predicted for a motor neuron releasing a fast-acting neurotransmitter.
346 Instead, HSN makes and releases the neuromodulator serotonin which signals through G
347 protein coupled serotonin receptors to activate the vulval muscles (Desai et al., 1988; Shyn et
348 al., 2003; Carnell et al., 2005; Hobson et al., 2006; Hapiak et al., 2009). The HSNs also
349 release serotonin onto the AVF interneurons in the nerve ring to promote a state of locomotion
350 arousal that accompanies the active state (Hardaker et al., 2001). Animals defective in
351 serotonin signaling have reduced egg laying (Tanis et al., 2008), but this defect is not as
352 severe as that of *egl-1(dm)* animals missing HSNs (Trent et al., 1983), suggesting HSN
353 releases additional neurotransmitters. We found that optogenetic activation of HSNs leads to

354 rhythmic activity of VC neurons, which are not known to express serotonin receptors, so an
355 unknown signal derived from HSN could directly activate VCs, as depicted in the Figure 7
356 model.

357 How is HSN activity controlled? The HSNs receive little synaptic input near the vulval
358 except from the PLM mechanosensory neurons (White, J.G. et al., 1986). The PLMs inhibit
359 HSN activity and egg laying in response to gentle touch (Zhang et al., 2008), but recent work
360 indicates the PLM neurons are also deformed during normal patterns of locomotion that could
361 contribute to rhythmic activity seen in HSN during egg laying (Topalidou et al., 2012).
362 Neuroendocrine signaling also regulates HSN activity. *flp-10* and *flp-17* neuropeptides are
363 released from the CO_2-responsive BAG neurons in the head, and these neuropeptides signal
364 through EGL-6 receptor and $G\alpha_o$ to activate IRK channels that inhibit HSN activity and egg
365 laying (Ringstad and Horvitz, 2008; Hallem et al., 2011; Emtage et al., 2012). Because loss of
366 EGL-6 or IRK channels do not increase egg laying as much as cell-specific inhibition of $G\alpha_o$,
367 there must be additional receptors and effectors of $G\alpha_o$ that inhibit HSN activity. $G\alpha_q$ signaling
368 opposes $G\alpha_o$ to increase serotonin release from the HSNs (Tanis et al., 2008), but the ligands
369 and receptors that activate $G\alpha_q$ have not yet been identified. Because we find that HSN Ca^{2+}
370 transients vary more in frequency than amplitude, we propose that these diverse sensory
371 signals increase or reduce the probability that HSN reaches a threshold potential that can
372 initiate, sustain, or terminate HSN activity and thus the active behavior state of the egg-laying
373 circuit.

374 We have also identified an HSN-independent mechanism that induces the active state.
375 Mutants lacking HSNs are strongly egg-laying defective, but eventually enter active states with
376 properly phased vulval muscle twitching and egg-laying transients. The active state was

377 eliminated in animals sterilized by FUDR, reducing vulval muscle activity and phasing to that
378 seen in the inactive state. Recent work has identified the gonad as an important site of
379 regulation for adult-specific behaviors in *C. elegans* (Fujiwara et al., 2016). We propose that
380 the accumulation of unlaid eggs in the uterus, perhaps leading to mechanical stretch, provides
381 an essential, permissive signal for entry into the active state. Several steps during embryo
382 production and maturation could regulate entry into the active state to result in the ~20 period
383 of the egg-laying inactive state.. Animals grown on food generate one new oocyte from each of
384 two gonad arms every ~10 minutes, balancing out the 3-5 eggs laid in the ~2 minute active
385 state that occurs every ~20 minutes, to result in a ~constant number of unlaid eggs in the
386 uterus (McCarter et al., 1999). New embryos are moved by gonadal sheath contractions into
387 the spermatheca for fertilization and deposition into the uterus. Excitable cells drive each of
388 these steps, providing potential sources of regulation by cell signaling and sensory feedback
389 (Kariya et al., 2004). Eight uterine muscles line the uterine lumen and form gap junctions with
390 the vm2 muscles (White, J.G. et al., 1986), and the addition of unlaid eggs into the uterus
391 could induce a mechanical stretch that cross-excites the vm2 muscles. Future work will be
392 required to understand how the accumulation of unlaid eggs promotes the active state.

393 Our results strongly imply that acetylcholine released from the VC motor neurons slows
394 locomotion during vulval muscle contraction. We found that animal locomotion slows during
395 egg release, and that optogenetic activation of the VC neurons halts movement and results in
396 body wall muscle contraction and animal shortening. This function of the VCs is likely via
397 acetylcholine signaling through nicotinic receptors expressed on ventral body wall muscles and
398 neurons that regulate locomotion (White, J.G. et al., 1986; Nagel et al., 2005). The effect of VC
399 activity to slow locomotion and contract body wall muscles may help compress the body and

400 uterus to encourage expulsion of eggs, analogous to the role of body wall muscle contraction in
401 facilitating defecation (Liu and Thomas, 1994).

402 Our results provide more complex evidence as to whether VC acetylcholine also directly
403 triggers egg release. We found that VC activity always accompanies egg-laying contractions of
404 the vulval muscles. The vulval muscles also express nicotinic acetylcholine receptors, and
405 receptor agonists including levamisole and nicotine stimulate egg laying (Weinshenker et al.,
406 1995; Waggoner et al., 2000). However, we found little correlation between the strength of the
407 VC activity and whether an egg is laid (Figure 1H), and that optogenetic activation of the VC
408 neurons fails to drive egg laying. Further, VC-defective and acetylcholine-deficient mutants
409 have *increased* egg-laying behavior (Bany et al., 2003; Ringstad and Horvitz, 2008). These
410 data together are consistent with a model in which acetylcholine released from the VA/VB
411 motor neurons signal through nicotinic receptors on the vm1 muscles to stimulate rhythmic
412 vulval muscle twitching, which combined with acetylcholine released from the VC neurons to
413 similarly excite the vm2 muscles results in egg laying. High levels of VC activity, such as
414 occurs during optogenetic activation, may drive release of additional signals, such as
415 neuropeptides, that inhibit egg-laying circuit activity (Bany et al., 2003; Banerjee et al., 2016),
416 or by freezing locomotion may feedback to halt the VA/VB activity required to drive vm1
417 contraction.

418 How is VC activity controlled? The VC neurons are unusual in that they are largely
419 presynaptic, only receiving input from each other and the HSNs. As noted above, optogenetic
420 activation of HSNs results in VC activity, suggesting a currently unknown signal from HSN
421 directly activates VCs. A second possible input onto VCs is suggested by the fact that the VC
422 neurons extend processes devoid of synapses dorsally along the vulval hypodermis that could

423 be mechanosensory (White, J.G. et al., 1986). Thus, rhythmic VC activity could be stimulated
424 mechanically by body bends or by a humoral signal released from the locomotor circuit (Hu et
425 al., 2011). Further, VC activity could be mechanically stimulated by vulval muscle contraction
426 (Zhang et al., 2010), particularly as we observed mechanical deformation of VC presynaptic
427 termini during strong twitching and egg-laying contractions. In this way, the VCs could act like
428 baroreceptors–mechanically activated by vulval muscle contraction to drive contraction of the
429 body wall muscles that results in animal slowing until the feedback of egg release. In this
430 model, the coordination of locomotion and egg laying by tying both behaviors to the same
431 central pattern generator allows productive egg release.

432 The uv1 neuroendocrine cells inform the circuit that eggs have been successfully laid.
433 Passage of eggs through the vulva mechanically deforms the uv1 cells and triggers a strong
434 Ca^{2+} transient. Our results suggest this activates uv1 to release tyramine that inhibits egg-
435 laying, at least in part via the LGC-55 receptor on the HSN neurons. Active states last ~2
436 minutes, and inhibitory tyramine release from uv1 could provide a feedback signal that
437 terminates activity in the circuit. The four uv1 cells have a unique structural position in the
438 vulva that may explain how they become activated during egg laying (Newman et al., 1996).
439 uv1 cells extend processes that contact and make adherens junctions with the ventral vulF
440 vulval cells. uv1 cells also makes dorsal attachments to utse, a large, H-shaped multinucleate
441 uterine seam cell that attaches the uterus to the lateral epidermis and that functions as a
442 hymen broken by the first egg-laying event. The acute mechanical strain on vulF, uv1, and/or
443 utse during egg passage could mechanically activate ion channels. Previous work has shown
444 uv1 expresses several TRPV channels that may be mechanosensory and contribute to this
445 response (Jose et al., 2007). A dominant-negative OCR-2 mutant expressed in uv1 leads to

446 hyperactive egg-laying behavior phenotype. We still observe Ca^{2+} transients in uv1 after egg-
447 laying events in this *ocr-2(vs29)* mutant (data not shown), suggesting other channels contribute
448 to the uv1 activity we see after egg laying. Although our results indicate that uv1 releases
449 tyramine to inhibit the HSNs via LGC-55, this signaling event does not fully explain the ability of
450 uv1 cells to inhibit the egg-laying circuit. We found that inhibition of egg laying by exogenous
451 tyramine is reduced but not eliminated in *lgc-55* null mutants, suggesting other tyramine
452 receptors help terminate the active state. The uv1 cells also make *nlp-7* and *flp-11*, two
453 neuropeptides that inhibit HSN activity and egg-laying behavior (Banerjee et al., submitted),
454 and the identification of the receptors and signaling pathways through which they inhibit
455 serotonin release will help to more fully understand how activity of the egg-laying circuit is
456 terminated.

457 Every neural circuit may require specific signals to initiate activity when its function is
458 required, signals to coordinate the dynamic activity of its various cells, and mechanisms to
459 determine when the circuit has successfully completed its task and signal to turn off activity.
460 Many circuits also must respond to specific signals from central pattern generators that
461 coordinate the activity of multiple circuits. A great challenge is to reduce these abstract
462 concepts to concrete, specific mechanisms in the case of a real circuit. For the *C. elegans* egg-
463 laying circuit, signals in each of the categories outlined above are now identified, albeit in
464 varying levels of detail and completeness. Continuing analysis of the *C. elegans* egg-laying
465 circuit using recordings of Ca^{2+} activity in behaving animals, combined with genetic,
466 optogenetic, and pharmacological manipulation, provides a path towards detailed
467 understanding the mechanisms that control activity of this model circuit.

468

469 **Materials and Methods**

470 Nematode Culture, Strains, and Maintenance

471 *Caenorhabditis elegans* strains were maintained as hermaphrodites at 20°C on Nematode
472 Growth Medium (NGM) agar plates with *E. coli* OP50 as a source of food as described
473 (Brenner, 1974). All strains are derived from the Bristol N2 wild-type strain, and all assays
474 were performed using age-matched adult hermaphrodites ~24 hours past the late L4 stage.
475 Animals were treated with 0.1 mg/ml floxuridine (FUDR) at a late L4 stage when all non-
476 germline cell divisions are complete. A list of strains, mutants, and transgenes used in this
477 study can be found in Table 1.

478 Molecular Biology and Transgenes

479 *Vulval muscles:* GCaMP5G (Akerboom et al., 2012) and mCherry were expressed in the
480 vulval muscles from the *unc-103e* promoter as previously described (Collins and Koelle, 2013).
481 Briefly, pKMC274 (GCaMP5, 20ng/*µ*l) and pKMC257 (mCherry, 2ng/*µ*l) were co-injected along
482 with the pL15EK *lin-15* rescue plasmid (50ng/*µ*l) into LX1832 *lite-1(ce314), lin-15(n765ts)* X
483 animals. The GCaMP5/mCherry extrachromosomal transgene produced was chromosomally
484 integrated using UV/TMP mutagenesis, creating the integrated transgene *vsIs164*, and the
485 resulting transgenic animals were backcrossed to the LX1832 parental line six times.

486 *HSN:* GCaMP5G and mCherry were expressed in the HSN motor neurons using the *nlp-3*
487 promoter. mCherry and GCaMP5G coding sequences were ligated into pJB9 bearing the *nlp-3*
488 promoter and *nlp-3* 3' untranslated region, and the resulting plasmids (GCaMP5, pKMC300,
489 80ng/*µ*l; mCherry, pKMC299, 20ng/*µ*l) were co-injected with pL15EK (50ng/*µ*l) into LX1832
490 worms. The extrachromosomal transgene produced was integrated with UV/TMP, creating the

491 integrated transgene *vsIs183,* and the resulting transgenic animals were backcrossed to the
492 LX1832 parental line six times. The *wzIs30* transgene expressing Channelrhodopsin-2 from
493 the *egl-6* promoter has been described (Emtage et al., 2012).

494 *VC:* GCaMP5G and mCherry were expressed in the VC motor neurons using pKMC145, a
495 pDM4-based plasmid bearing a *lin-11* enhancer region fused to the *pes-10* basal promoter with
496 a modified multiple cloning site (Bany et al., 2003; Tanis et al., 2008). Derivatives expressing
497 GCaMP5 (pKMC273, 80ng/*µ*l) and mCherry (pKMC275, 30ng/*µ*l) were co-injected with
498 pL15EK (50ng/*µ*l) into LX1832 worms. The extrachromosomal transgene produced was
499 integrated with UV/TMP, creating the transgene *vsIs172*, and transgenic animals were
500 backcrossed to the LX1832 parental line six times. To activate the VCs optogenetically, coding
501 sequences for ChR2-YFP bearing the H134R, T159C mutations (Erbguth et al., 2012) were
502 amplified by PCR, ligated into pKMC145 to generate pKMC283, injected at 80ng/*µ*l into
503 LX1832 along with pL15EK at 50ng/*µ*l. The extrachromosomal transgene produced was
504 integrated with UV/TMP creating the transgene *keyIs3,* and the resulting animals were
505 backcrossed to LX1832 parental line six times.

506 *uv1:* GCaMP5G and mCherry were expressed in uv1 using the *ocr-2* promoter. GCaMP5 and
507 mCherry coding sequences were ligated into pJT79 between the *ocr-2* promoter and 3'
508 untranslated region (Jose et al., 2007) to generate plasmids pKMC281 and pKMC284,
509 respectively. Long-range PCR products amplified from these plasmids were injected into
510 worms at 80ng/*µ*l each along with pL15EK (50ng/*µ*l) as previously described (Jose et al., 2007).
511 The extrachromosomal transgene produced was integrated with UV/TMP creating the
512 transgene *vsIs177*, and the resulting animals were backcrossed to the LX1832 parental line six
513 times.

514 *lgc-55*: A ~40 kb genomic fosmid clone (WRM063D_A12; Perkins, 2011) recombineered to
515 express LGC-55 tagged with GFP at the C-terminus (Sarov et al., 2012) was injected at
516 100ng/μl into LX2081 *unc-119(ed3)* mutant animals expressing TagRFP pan-neuronally to
517 generate the strain LX2126. These animals were then crossed with LX2096 animals to
518 exchange pan-neural mCherry transgene for one that expresses in the vulval muscles,
519 generating LX2126. Fluorescence was visualized on immobilized animals with a 63x water
520 objective on a Zeiss LSM 710 Duo confocal microscope. For cell-specific rescue, LGC-55 was
521 expressed in the HSN neurons of *lgc-55* mutant animals using the *tph-1* promoter. Briefly, a
522 *lgc-55* cDNA (Pirri et al., 2009) was inserted into pJM66A plasmid (Moresco and Koelle, 2004)
523 to generate pJT105. pJT105, or a GFP-expressing control plasmid (pJM60A), was injected at
524 100ng/μl along with pL15EK rescue plasmid (50ng/μl) into *lgc-55(tm2913); lin-15(n765ts)*
525 double mutant animals. Egg-laying behavior was analyzed in five independent transgenic lines
526 expressing LGC-55 or GFP, and one strain each were kept for long-term storage.

527 Ratiometric Ca^{2+} Imaging

528 Animals were mounted between glass coverslips and chunked sections of NGM plates for
529 imaging as described (Collins and Koelle, 2013; Li et al., 2013). The stage and focus were
530 adjusted manually to keep the egg-laying system in view during recording periods. Three
531 different imaging systems were used to collect recordings, and each gave quantitatively similar
532 results. First, single, two-channel confocal slices (18 μm thick) of GCaMP5 and mCherry
533 fluorescence were collected through a 20x Plan Apochromat objective (0.8NA) using a Zeiss
534 Axio Observer microscope and recorded at 20 fps at 256x256 pixel resolution, 16-bit depth
535 using a 710 Duo LIVE scanner as described previously (Collins and Koelle, 2013; Li et al.,
536 2013). Second, widefield GCaMP5 and mCherry fluorescence was imaged through a 20x Plan

537 Apochromat objective (0.8NA) using a Zeiss Axio Observer microscope, and the GCaMP5 and
538 mCherry fluorescence was separated using a W-View Gemini image splitter at 20 fps at
539 256x256 pixel resolution, 16-bit depth onto a single, 4x4 binned Hamamatsu ORCA Flash 4.0
540 V2 sCMOS sensor after excitation with 470 nm and 590 nm LEDs (Zeiss Colibri.2). Third,
541 single, two-channel confocal slices (20 μm thick) of GCaMP5 and mCherry fluorescence were
542 collected using an inverted Leica TCS SP5 confocal microscope with the resonant scanner
543 running at 8,000Hz and collected at 20 fps at 256x256 pixel resolution, 12-bit depth after 2x
544 digital zoom.

545 Quantitative ratiometric analysis was performed after importing image sequences into
546 Volocity (Perkin Elmer). GCaMP5/mCherry ratios were calculated, and pixels with mCherry
547 fluorescence intensities ~2 standard deviations above background were selected as objects for
548 mean ratio measurement. While the Volocity algorithm set with these parameters typically
549 identified the vulval muscles and uv1 cells as a single object, the complex morphology of the
550 HSN and VC neurons often led to the cells being found as two or more objects within each
551 video frame. These were rejoined using a custom script in MATLAB (Mathworks). The ratio of
552 the joined object was scaled in proportion to the area of each component object to generate an
553 area-adjusted GCaMP5/mCherry ratio. The ratio data were then smoothed using a 150 msec
554 (three timepoint) rolling average, and the lowest 10% of the GCaMP5/mCherry ratio values
555 over the entire recording period were averaged to establish a $\Delta R/R$ baseline. Ca^{2+} transients
556 and their features (peak amplitude and width at half-maximum) were identified from ratio traces
557 using the *findpeaks* algorithm in MATLAB, and peaks were confirmed by visual inspection of
558 GCaMP5/mCherry recordings and ratio traces. Egg-laying events were observed by allowing a
559 small amount of bright field light to transmit into the mCherry channel whose gain was

560 increased for egg visualization. The egg-laying active state was defined in recordings to
561 include those transients that occurred one minute before and one minute after each egg-laying
562 event. Those transients not found within an active state were considered to be in the inactive
563 state. To facilitate comparisons of ΔR/R between different reporters and recording conditions
564 (Figure 1H and 5D), the maximum peak amplitude was normalized to 1. For phasing analysis,
565 the timing of individual Ca^{2+} transient peaks relative to ventral relaxation and contraction was
566 determined independent of whether the animal was engaged in forward or reverse locomotion,
567 as described previously (Collins and Koelle, 2013).

568 Optogenetics

569 Channelrhodopsin-2 (ChR2) expressing strains were grown in the presence or absence of the
570 ChR2 cofactor all-*trans* retinal (ATR). ATR was prepared at 100mM in 100% ethanol and
571 stored at -20°C. To prepare NGM plates for behavior analysis, ATR was diluted to 0.4 mM with
572 warmed cultures of OP50 bacteria in B Broth, and 200 μl of culture was seeded onto each 60
573 mm NGM plate. The plates were allowed to grow for 24 hours at 25-37°C, after which late L4
574 worms were staged onto prepared plates for behavioral assays 24 hours later. During Ca^{2+}
575 imaging experiments, ChR2 was activated with the same light used for GCaMP5 excitation.
576 For timed behavior recording experiments on plates, a OTPG_4 TTL Pulse Generator (Doric
577 Optics) was used to trigger image capture (Grasshopper 3, 4.1 Megapixel, USB3 CMOS
578 camera, Point Grey Research) and shutter opening on a EL6000 metal halide light source
579 generating 8-16 mW/cm^2 (depending on the magnification used) of ~470±20nm blue light via a
580 EGFP filter set mounted on a Leica M165FC stereomicroscope. Worm size, speed, and body
581 bends were determined from image sequences using Volocity.

582 Tyramine behavior assays

583 Three adult animals were placed onto each of three 35 mm agar plates prepared with
584 tyramine-HCl (Sigma) and acetic acid seeded with OP50 bacteria as described (Pirri et al.,
585 2009). The average number of eggs laid was counted after 30 minutes from at least 11 trials
586 for each genotype and tyramine concentration.

587 Statistical analyses

588 Data were analyzed using Prism 6 (GraphPad). Average worm speed, worm length, body
589 bends, or eggs laid were compared using one-way ANOVA with Bonferroni correction for
590 multiple comparisons, and error bars indicate 95% confidence intervals for the mean. Ca^{2+}
591 transient peak amplitudes, widths, and inter-transient intervals were pooled from multiple
592 animals ($n \geq 5$ animals per experiment), compared using the Mann-Whitney test (for pair-wise
593 comparisons) or the Kruskal-Wallis test with Dunn's correction (for multiple comparisons), and
594 error bars indicate quartile intervals for the indicated median. $p<0.05$ interactions were deemed
595 significant and are labeled with an asterisk.

596

Acknowledgments

This work was funded by a postdoctoral fellowship from the American Heart Association to KMC (POST4990016) and by grants from the NINDS to MRK (NS036918) and to MRK and KMC (NS086932). Confocal instrumentation was supported by a grant to the Yale Liver Center (DK34989). Some strains were provided by the *C. elegans* Genetics Center, which is funded by NIH Office of Research Infrastructure Programs (P40 OD010440). We thank members of the Koelle and Collins labs, and Drs. James Baker, Julia Dallman, and Mason Klein for comments and helpful discussions on the manuscript.

Competing Interests

The authors declare no financial and non-financial competing interests.

609 **References**

610 Akerboom J et al. (2012) Optimization of a GCaMP calcium indicator for neural activity imaging.
611 J Neurosci Off J Soc Neurosci 32:13819–13840.

612 Alkema MJ, Hunter-Ensor M, Ringstad N, Horvitz HR (2005) Tyramine Functions
613 independently of octopamine in the Caenorhabditis elegans nervous system. Neuron
614 46:247–260.

615 Bany IA, Dong M-Q, Koelle MR (2003) Genetic and cellular basis for acetylcholine inhibition of
616 Caenorhabditis elegans egg-laying behavior. J Neurosci Off J Soc Neurosci 23:8060–
617 8069.

618 Bellemer A, Hirata T, Romero MF, Koelle MR (2011) Two types of chloride transporters are
619 required for GABA(A) receptor-mediated inhibition in C. elegans. EMBO J 30:1852–
620 1863.

621 Brenner S (1974) The genetics of Caenorhabditis elegans. Genetics 77:71–94.

622 Brundage L, Avery L, Katz A, Kim UJ, Mendel JE, Sternberg PW, Simon MI (1996) Mutations
623 in a C. elegans Gqalpha gene disrupt movement, egg laying, and viability. Neuron
624 16:999–1009.

625 Carnell L, Illi J, Hong SW, McIntire SL (2005) The G-protein-coupled serotonin receptor SER-1
626 regulates egg laying and male mating behaviors in Caenorhabditis elegans. J Neurosci
627 Off J Soc Neurosci 25:10671–10681.

628 Collins KM, Koelle MR (2013) Postsynaptic ERG Potassium Channels Limit Muscle Excitability
629 to Allow Distinct Egg-Laying Behavior States in Caenorhabditis elegans. J Neurosci Off
630 J Soc Neurosci 33:761–775.

631 Daniels SA, Ailion M, Thomas JH, Sengupta P (2000) egl-4 acts through a transforming growth
632 factor-beta/SMAD pathway in Caenorhabditis elegans to regulate multiple neuronal
633 circuits in response to sensory cues. Genetics 156:123–141.

634 Desai C, Garriga G, McIntire SL, Horvitz HR (1988) A genetic pathway for the development of
635 the Caenorhabditis elegans HSN motor neurons. Nature 336:638–646.

636 Dong MQ, Chase D, Patikoglou GA, Koelle MR (2000) Multiple RGS proteins alter neural G
637 protein signaling to allow C. elegans to rapidly change behavior when fed. Genes Dev
638 14:2003–2014.

639 Elkes DA, Cardozo DL, Madison J, Kaplan JM (1997) EGL-36 Shaw channels regulate C.
640 elegans egg-laying muscle activity. Neuron 19:165–174.

641 Emtage L, Aziz-Zaman S, Padovan-Merhar O, Horvitz HR, Fang-Yen C, Ringstad N (2012)
642 IRK-1 Potassium Channels Mediate Peptidergic Inhibition of Caenorhabditis elegans
643 Serotonin Neurons via a Go Signaling Pathway. J Neurosci Off J Soc Neurosci
644 32:16285–16295.

645 Erbguth K, Prigge M, Schneider F, Hegemann P, Gottschalk A (2012) Bimodal activation of
646 different neuron classes with the spectrally red-shifted channelrhodopsin chimera C1V1
647 in Caenorhabditis elegans. PloS One 7:e46827.

648 Fujiwara M, Aoyama I, Hino T, Teramoto T, Ishihara T (2016) Gonadal Maturation Changes
649 Chemotaxis Behavior and Neural Processing in the Olfactory Circuit of Caenorhabditis
650 elegans. Curr Biol CB 26:1522–1531.

651 Hajdu-Cronin YM, Chen WJ, Patikoglou G, Koelle MR, Sternberg PW (1999) Antagonism
652 between G(o)alpha and G(q)alpha in Caenorhabditis elegans: the RGS protein EAT-16
653 is necessary for G(o)alpha signaling and regulates G(q)alpha activity. Genes Dev
654 13:1780–1793.

655 Hallem EA, Spencer WC, McWhirter RD, Zeller G, Henz SR, Rätsch G, Miller DM, Horvitz HR,
656 Sternberg PW, Ringstad N (2011) Receptor-type guanylate cyclase is required for
657 carbon dioxide sensation by Caenorhabditis elegans. Proc Natl Acad Sci U S A
658 108:254–259.

659 Hapiak VM, Hobson RJ, Hughes L, Smith K, Harris G, Condon C, Komuniecki P, Komuniecki
660 RW (2009) Dual excitatory and inhibitory serotonergic inputs modulate egg laying in
661 Caenorhabditis elegans. Genetics 181:153–163.

662 Hardaker LA, Singer E, Kerr R, Zhou G, Schafer WR (2001) Serotonin modulates locomotory
663 behavior and coordinates egg-laying and movement in Caenorhabditis elegans. J
664 Neurobiol 49:303–313.

665 Hobson RJ, Hapiak VM, Xiao H, Buehrer KL, Komuniecki PR, Komuniecki RW (2006) SER-7,
666 a Caenorhabditis elegans 5-HT7-like receptor, is essential for the 5-HT stimulation of
667 pharyngeal pumping and egg laying. Genetics 172:159–169.

668 Hu Z, Pym ECG, Babu K, Vashlishan Murray AB, Kaplan JM (2011) A neuropeptide-mediated
669 stretch response links muscle contraction to changes in neurotransmitter release.
670 Neuron 71:92–102.

671 Johnstone DB, Wei A, Butler A, Salkoff L, Thomas JH (1997) Behavioral defects in C. elegans
672 egl-36 mutants result from potassium channels shifted in voltage-dependence of
673 activation. Neuron 19:151–164.

674 Jose AM, Bany IA, Chase DL, Koelle MR (2007) A specific subset of transient receptor
675 potential vanilloid-type channel subunits in Caenorhabditis elegans endocrine cells
676 function as mixed heteromers to promote neurotransmitter release. Genetics 175:93–
677 105.

678 Jospin M, Jacquemond V, Mariol M-C, Segalat L, Allard B (2002) The L-type voltage-
679 dependent Ca2+ channel EGL-19 controls body wall muscle function in Caenorhabditis
680 elegans. J Cell Biol 159:337–348.

681 Kariya K-I, Bui YK, Gao X, Sternberg PW, Kataoka T (2004) Phospholipase Cepsilon regulates
682 ovulation in Caenorhabditis elegans. Dev Biol 274:201–210.

683 Kim J, Poole DS, Waggoner LE, Kempf A, Ramirez DS, Treschow PA, Schafer WR (2001)
684 Genes affecting the activity of nicotinic receptors involved in Caenorhabditis elegans
685 egg-laying behavior. Genetics 157:1599–1610.

686 Koelle MR, Horvitz HR (1996) EGL-10 regulates G protein signaling in the C. elegans nervous
687 system and shares a conserved domain with many mammalian proteins. Cell 84:115–
688 125.

689 Lee RY, Lobel L, Hengartner M, Horvitz HR, Avery L (1997) Mutations in the alpha1 subunit of
690 an L-type voltage-activated Ca2+ channel cause myotonia in Caenorhabditis elegans.
691 EMBO J 16:6066–6076.

692 Li P, Collins KM, Koelle MR, Shen K (2013) LIN-12/Notch signaling instructs postsynaptic
693 muscle arm development by regulating UNC-40/DCC and MADD-2 in Caenorhabditis
694 elegans. eLife 2:e00378.

695 Liu DW, Thomas JH (1994) Regulation of a periodic motor program in C. elegans. J Neurosci
696 Off J Soc Neurosci 14:1953–1962.

697 Marder E (2012) Neuromodulation of neuronal circuits: back to the future. Neuron 76:1–11.

698 Marder E, Goeritz ML, Otopalik AG (2015) Robust circuit rhythms in small circuits arise from
699 variable circuit components and mechanisms. Curr Opin Neurobiol 31:156–163.

700 McCarter J, Bartlett B, Dang T, Schedl T (1999) On the control of oocyte meiotic maturation
701 and ovulation in Caenorhabditis elegans. Dev Biol 205:111–128.

702 Miller KG, Emerson MD, Rand JB (1999) Goalpha and diacylglycerol kinase negatively
703 regulate the Gqalpha pathway in C. elegans. Neuron 24:323–333.

704 Mitchell DH, Stiles JW, Santelli J, Sanadi DR (1979) Synchronous growth and aging of
705 Caenorhabditis elegans in the presence of fluorodeoxyuridine. J Gerontol 34:28–36.

706 Moresco JJ, Koelle MR (2004) Activation of EGL-47, a Galpha(o)-coupled receptor, inhibits
707 function of hermaphrodite-specific motor neurons to regulate Caenorhabditis elegans
708 egg-laying behavior. J Neurosci Off J Soc Neurosci 24:8522–8530.

709 Nagel G, Brauner M, Liewald JF, Adeishvili N, Bamberg E, Gottschalk A (2005) Light activation
710 of channelrhodopsin-2 in excitable cells of Caenorhabditis elegans triggers rapid
711 behavioral responses. Curr Biol CB 15:2279–2284.

712 Newman AP, Sternberg PW (1996) Coordinated morphogenesis of epithelia during
713 development of the Caenorhabditis elegans uterine-vulval connection. Proc Natl Acad
714 Sci 93:9329–9333.

715 Newman AP, White JG, Sternberg PW (1996) Morphogenesis of the C. elegans hermaphrodite
716 uterus. Dev Camb Engl 122:3617–3626.

717 Perkins, Jaryn Daniel (2011) Comparison of fosmid libraries made from two geographic
718 isolates of Caenorhabditis elegans. Available at: http://dx.doi.org/10.14288/1.0071587
719 [Accessed August 6, 2016].

720 Pirri JK, McPherson AD, Donnelly JL, Francis MM, Alkema MJ (2009) A tyramine-gated
721 chloride channel coordinates distinct motor programs of a Caenorhabditis elegans
722 escape response. Neuron 62:526–538.

723 Porter MY, Xie K, Pozharski E, Koelle MR, Martemyanov KA (2010) A Conserved Protein
724 Interaction Interface on the Type 5 G Protein β Subunit Controls Proteolytic Stability and
725 Activity of R7 Family Regulator of G Protein Signaling Proteins. J Biol Chem
726 285:41100–41112.

727 Ringstad N, Horvitz HR (2008) FMRFamide neuropeptides and acetylcholine synergistically
728 inhibit egg-laying by C. elegans. Nat Neurosci 11:1168–1176.

729 Sarov M et al. (2012) A genome-scale resource for in vivo tag-based protein function
730 exploration in C. elegans. Cell 150:855–866.

731 Schafer WF (2006) Genetics of egg-laying in worms. Annu Rev Genet 40:487–509.

732 Shyn SI, Kerr R, Schafer WR (2003) Serotonin and Go modulate functional states of neurons
733 and muscles controlling C. elegans egg-laying behavior. Curr Biol CB 13:1910–1915.

734 Tanis JE, Bellemer A, Moresco JJ, Forbush B, Koelle MR (2009) The potassium chloride
735 cotransporter KCC-2 coordinates development of inhibitory neurotransmission and
736 synapse structure in Caenorhabditis elegans. J Neurosci Off J Soc Neurosci 29:9943–
737 9954.

738 Tanis JE, Moresco JJ, Lindquist RA, Koelle MR (2008) Regulation of serotonin biosynthesis by
739 the G proteins Galphao and Galphaq controls serotonin signaling in Caenorhabditis
740 elegans. Genetics 178:157–169.

741 Topalidou I, Keller C, Kalebic N, Nguyen KCQ, Somhegyi H, Politi KA, Heppenstall P, Hall DH,
742 Chalfie M (2012) Genetically separable functions of the MEC-17 tubulin
743 acetyltransferase affect microtubule organization. Curr Biol CB 22:1057–1065.

744 Trent C, Tsuing N, Horvitz HR (1983) Egg-laying defective mutants of the nematode
745 Caenorhabditis elegans. Genetics 104:619–647.

746 Waggoner LE, Dickinson KA, Poole DS, Tabuse Y, Miwa J, Schafer WR (2000) Long-term
747 nicotine adaptation in Caenorhabditis elegans involves PKC-dependent changes in
748 nicotinic receptor abundance. J Neurosci Off J Soc Neurosci 20:8802–8811.

749 Waggoner LE, Zhou GT, Schafer RW, Schafer WR (1998) Control of alternative behavioral
750 states by serotonin in Caenorhabditis elegans. Neuron 21:203–214.

751 Weinshenker D, Garriga G, Thomas JH (1995) Genetic and pharmacological analysis of
752 neurotransmitters controlling egg laying in C. elegans. J Neurosci Off J Soc Neurosci
753 15:6975–6985.

754 Weinshenker D, Wei A, Salkoff L, Thomas JH (1999) Block of an ether-a-go-go-like K(+)
755 channel by imipramine rescues egl-2 excitation defects in Caenorhabditis elegans. J
756 Neurosci Off J Soc Neurosci 19:9831–9840.

757 White JG, Southgate E, Thomson JN, Brenner S (1976) The structure of the ventral nerve cord
758 of Caenorhabditis elegans. Philos Trans R Soc Lond B Biol Sci 275:327–348.

759 White, J.G., Southgate, E., Thomson, J.N., Brenner, S. (1986) The structure of the nervous
760 system of the nematode Caenorhabditis elegans. Phil Trans R Soc 314:1–340.

761 Williams SL, Lutz S, Charlie NK, Vettel C, Ailion M, Coco C, Tesmer JJG, Jorgensen EM,
762 Wieland T, Miller KG (2007) Trio's Rho-specific GEF domain is the missing Galpha q
763 effector in C. elegans. Genes Dev 21:2731–2746.

764 Zhang M, Chung SH, Fang-Yen C, Craig C, Kerr RA, Suzuki H, Samuel ADT, Mazur E,
765 Schafer WR (2008) A self-regulating feed-forward circuit controlling C. elegans egg-
766 laying behavior. Curr Biol CB 18:1445–1455.

767 Zhang M, Schafer WR, Breitling R (2010) A circuit model of the temporal pattern generator of
768 Caenorhabditis egg-laying behavior. BMC Syst Biol 4:81.

769

770

771 **Table 1: Strains used in this study**

Strain	Feature	Genotype	Figures
LX1832	Strain for transgene production	*lite-1(ce314) lin-15(n765ts)* X	1-6
LX1836	HSN Channelrhodopsin	*wzIs30* IV; *lite-1(ce314) lin-15(n765ts)* X	3
LX1918	vulval muscle GCaMP5, mCherry	*lite-1(ce314) vsIs164 lin-15(n765ts)* X	1, 2, 3
LX1932	HSN Channelrhodopsin, vulval muscle GCaMP5, mCherry	*wzIs30* IV; *lite-1(ce314) vsIs164 lin-15(n765ts)* X	3
LX1938	No HSNs, vulval muscle GCaMP5, mCherry	*egl-1(n986dm)* V; *lite-1(ce314) vsIs164 lin-15(n765ts)* X	4
LX1986	uv1 GCaMP5, mCherry	*vsIs177*; *lite-1(ce314) lin-15(n765ts)* X	5
LX1960	VC GCaMP5, mCherry	*vsIs172*; *lite-1(ce314) lin-15(n765ts)* X	1, 2
LX1970	HSN Channelrhodopsin, VC GCaMP5, mCherry	*wzIs30* IV; *vsIs172*; *lite-1(ce314) lin-15(n765ts)* X	3
LX2004	HSN GCaMP5, mCherry	*lite-1(ce314), vsIs183 lin-15(n765ts)* X	1, 2, 6
LX2038	*lgc-55* null mutant HSN GCaMP5, mCherry	*lgc-55(tm2913)* V *lite-1(ce314) vsIs183 lin-15(n765ts)* X	6
MIA3	VC Channelrhodopsin	*keyIs3*; *lite-1(ce314) lin-15(n765ts)* X	3
MT13113	*tdc-1* null mutant; no tyramine biosynthesis	*tdc-1(n3419)* II	6
N2	Bristol strain	wild type	6
OH313	*ser-2* null mutant	*ser-2(pk1357)* X	6
VC125	*tyra-3* null mutant	*tyra-3(ok325)* X	6
QW89	*lgc-55* null mutant	*lgc-55(tm2913)* V	6
LX2096	vulval muscle mCherry	*vsIs191; lin-15(n765ts)* X	
LX2081	pan-neuronal TagRFP	*unc-119(ed3)* I*; otIs356*	
LX2137	vulval muscle mCherry*, lgc-55::gfp*	*vsIs191*; *vsEx791*	6
LX1330	*lgc-55* mutant expressing GFP in HSN from *tph-1* promoter	*lgc-55(tm2913)* V*; lin-15(n765ts)* X *vsEx557*	6
LX1329	*lgc-55* mutant expressing LGC-55 in HSN from *tph-1* promoter	*lgc-55(thm2913)* V*; lin-15(n765ts)* X *vsEx558*	6

772

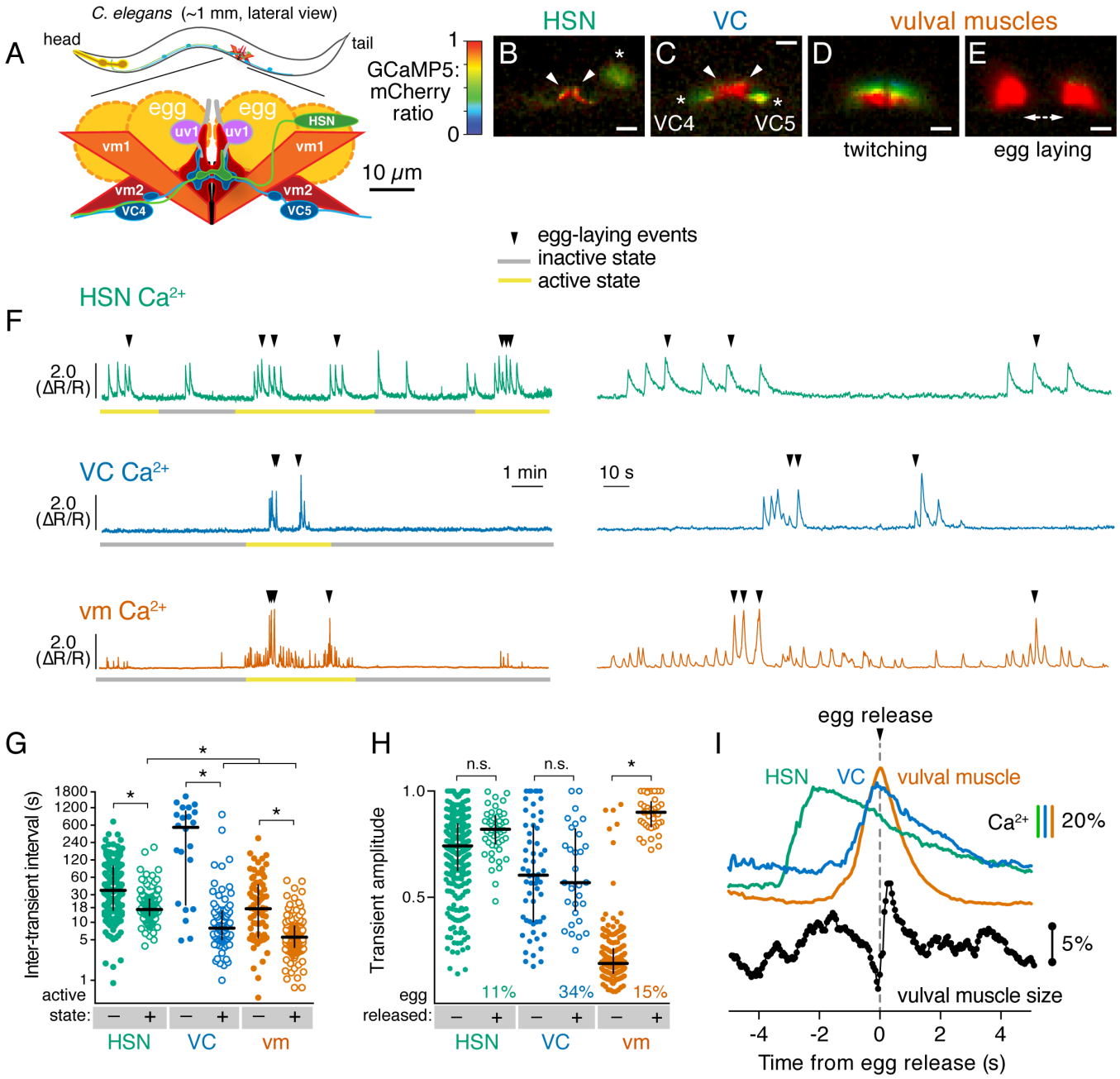

Figure 1. Cell-specific reporters of activity in the *C. elegans* egg-laying behavior circuit.

(**A**) Schematic of the circuit. HSN (green) and VC (blue) motor neurons synapse onto the vm2 muscle postsynaptic termini (center of schematic). The uv1 neuroendocrine cells (pink) extend processes (grey) along the vulval slit and vm2 postsynaptic terminus. (**B-E**) Individual video

778 frames of the GCaMP5:mCherry fluorescence ratio showing active state Ca^{2+} transients in
779 HSNs (**B**), VCs (**C**), and vulval muscles during twitching (**D**) and egg-laying behaviors (**E**).
780 Arrowheads, HSN and VC presynaptic termini; asterisks, cell bodies; scale bar, 10 μm. (**F**) 30
781 minute recordings of HSN, VC, and vulval muscle activity (left panel), showing distinct active
782 (yellow) and inactive (grey) egg-laying behavior states, with expanded timescale of one active
783 state at right. Arrowheads show egg-laying events. (**G**) Scatter plots and median HSN, VC, and
784 vulval muscle (vm) inter-transient intervals during egg-laying inactive (–, filled circles) and
785 active (+, open circles) states. Asterisks indicate significant differences (p<0.0001). (**H**)
786 Relationship between Ca^{2+} transient amplitude and egg release. Scatter plots and medians of
787 normalized amplitude with (+; open circles) and without (–; closed circles) egg release. Also
788 shown is the percent of total transients that accompanied egg release. (**I**) Timing of HSN, VC,
789 and vulval muscle Ca^{2+} transients and egg release. Shown at top is a curve of the median of
790 Ca^{2+} from HSN (green), VC (blue), and vulval muscles (orange) from normalized $\Delta R/R$ traces
791 (with the peak Ca^{2+} set to 100%) synchronized to the moment of egg release (0 s, arrowhead
792 and dotted line). Bars indicate 20% change in median GCaMP/mCherry ratio. The timing of the
793 HSN Ca^{2+} peak is significantly different from that of the VCs and vulval muscles (p<0.0001;
794 n≥31 egg-laying events). Shown at bottom is a trace of median vulval muscle size. Bar shows
795 a 5% change in median object size based on mCherry fluorescence.

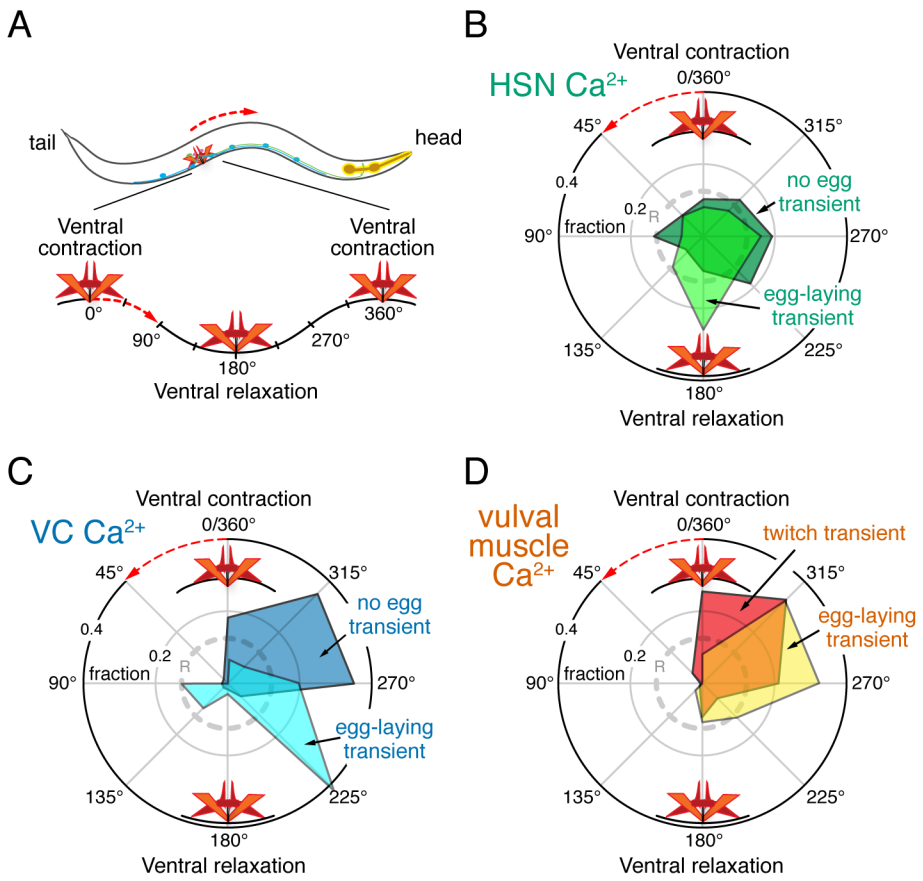

Figure 2. HSN, VC, and vulval muscle activity is phased with animal locomotion.

(**A**) The position of the vulva within a sinusoidal locomotor body bend at the moment a Ca^{2+} transient peaked was used to assign a body bend "phase", in units of degrees, for each Ca^{2+} transient observed in HSN (**B**), VC (**C**), and vulval muscle (**D**) for the recordings analyzed in Figure 1. The fraction of transients observed in each of eight 45° bins was plotted on a circular histogram with ventral relaxation at 180°, and ventral contraction at 0/360°. Ca^{2+} transients that resulted in egg release had significantly different phasing from those that did not (HSN, p=0.0058; VC, p=0.001; vulval muscles, p=0.0071; Mann-Whitney test). The phasing of HSN, VC, and vulval muscle transients is significantly different from a random distribution (R, dashed line at 0.125; p<0.05) except for those HSN transients that did not result in egg release.

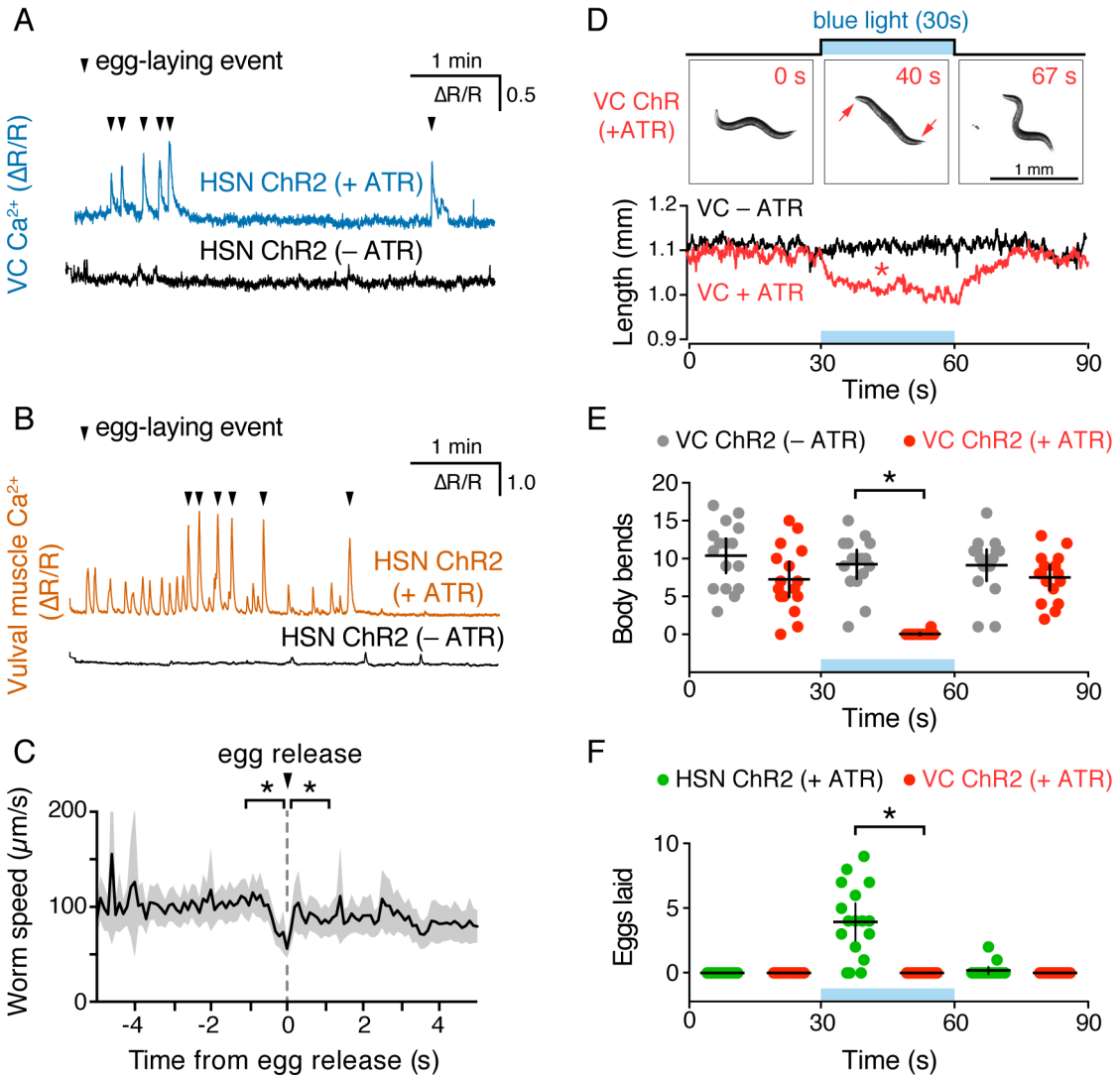

Figure 3. Optogenetic activation of HSN neurons initiates the egg-laying active state, and optogenetic activation of VC neurons slows locomotion.

(**A**) Animals expressing Channelrhodopsin-2 (ChR2) in the HSNs and GCaMP5/mCherry in the VC neurons were grown in the presence (+ATR; top, blue) or absence (–ATR; bottom, black) of all-*trans* retinal. 489 nm laser light was used to simultaneously stimulate ChR2 activity and excite GCaMP5 fluorescence during the entire recording. Arrowheads indicate egg-laying events. (**B**) The same experiment as (A) except that GCaMP5/mCherry were expressed in the

825 vulval muscles rather than VCs. (**C**) Brief reduction of animal speed during optogenetically-
826 induced egg laying. The egg-laying active state in animals expressing ChR2 in the HSN
827 neurons was induced with 30 s exposure to blue light. Average speed (black trace) about each
828 egg-laying event (0 s) was calculated from the worm centroid position, and the grey area
829 shows the 95% confidence interval. Average speed at the moment of egg laying release (0 s)
830 is reduced compared to 1 s before or after (p <0.001). See also Movie 4. (**D**) Activation of the
831 VC neurons slows locomotion but fails to induce egg laying. Animals expressing ChR2 in the
832 VCs were grown in the presence (+ATR; red) or absence (–ATR; black/grey) of all-*trans* retinal,
833 and worm length (upper photos and graph) was determined. Micrographs are still images from
834 a representative animal at indicated time points (see Movie 5). Inset arrows indicate regions of
835 the head and tail that remain mobile after VC activation. Scatter plots of body bends (**E**) and
836 egg laying (**F**) from the same recordings shown in D. There was a significant change in worm
837 length and body bends, but not egg laying, during blue light in animals grown on ATR (red;
838 p<0.0001; n=17 animals). Positive control animals expressing ChR2 in the HSNs (green)
839 showed a significant increase in egg laying during blue light (p<0.0001; n≥14 animals).

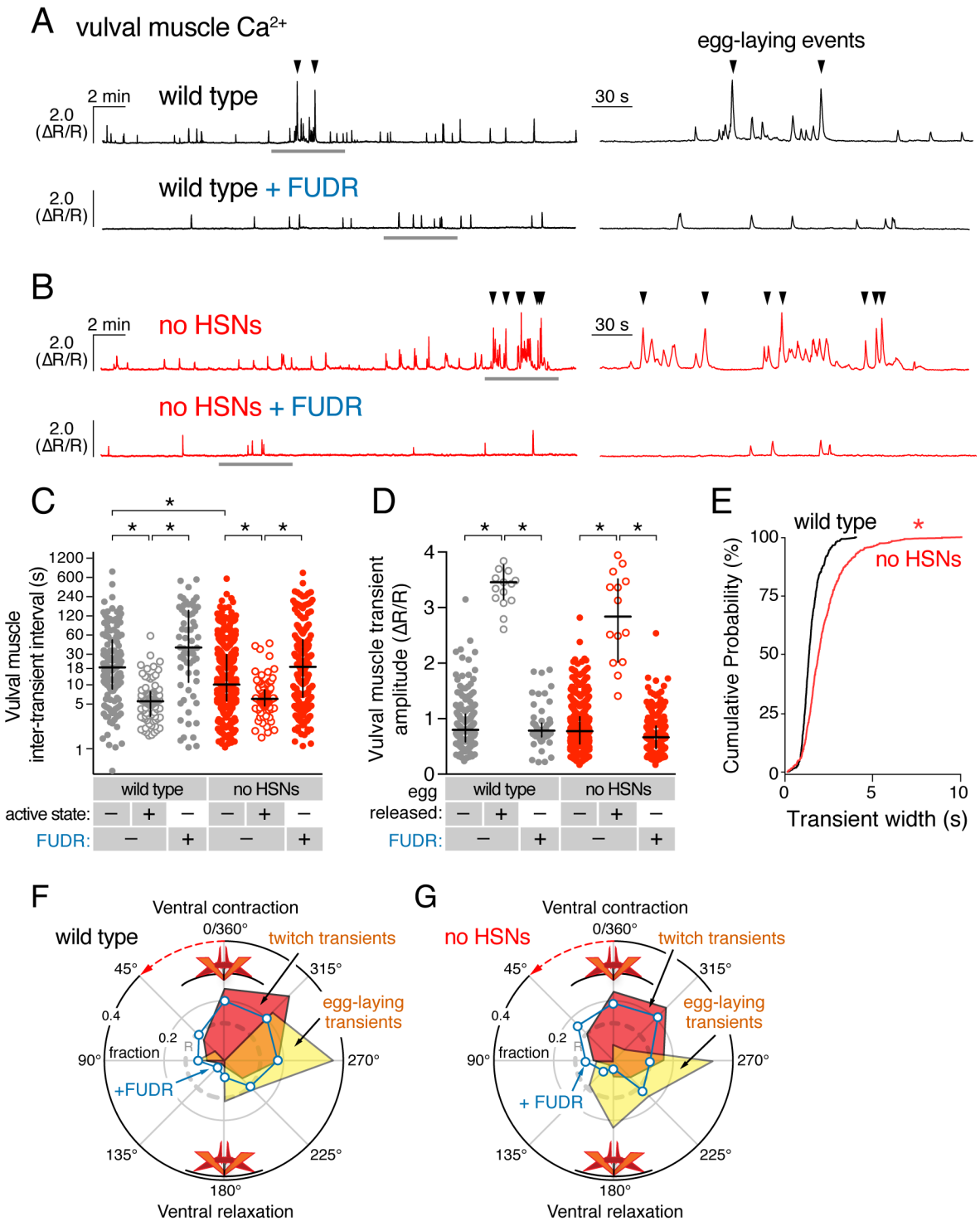

Figure 4. Active states require egg production but not the HSNs.

(**A**) Vulval muscle activity in wild-type animals either untreated or after sterilization with floxuridine (FUDR). Left panel shows 30-minute recordings with the grey underlined regions

844 expanded at right. (**B**) Vulval muscle activity in *egl-1(n986dm)* mutants lacking HSNs. (**C-D**)
845 Scatter plots of vulval muscle inter-transient intervals (**C**) and amplitudes (**D**). Line indicates
846 median, error bars indicate quartiles, and asterisks indicate significant differences ($p<0.01$). (**E**)
847 Vulval muscle transients are wider in animals lacking HSNs. Cumulative distribution plots of
848 Ca^{2+} transient peak widths; asterisk indicates $p<0.0001$ (Mann-Whitney test). **(F, G)** Vulval
849 muscle Ca^{2+} transient phasing after sterilization resembles that of the inactive state. The
850 relative timing of peak vulval muscle Ca^{2+} transients during twitching (red), egg-laying (yellow),
851 and after FUDR treatment (blue) are plotted as in Figure 2. Twitch, egg-laying, and FUDR Ca^{2+}
852 transient timings were significantly different from each other and from a random distribution (R,
853 dashed line at 0.125; $p<0.05$). (**F**) Transients from 14 untreated and 5 FUDR-treated wild-type
854 animals. (**G**) Transients from 23 untreated and 10 FUDR-treated *egl-1(n986dm)* animals.

855

856

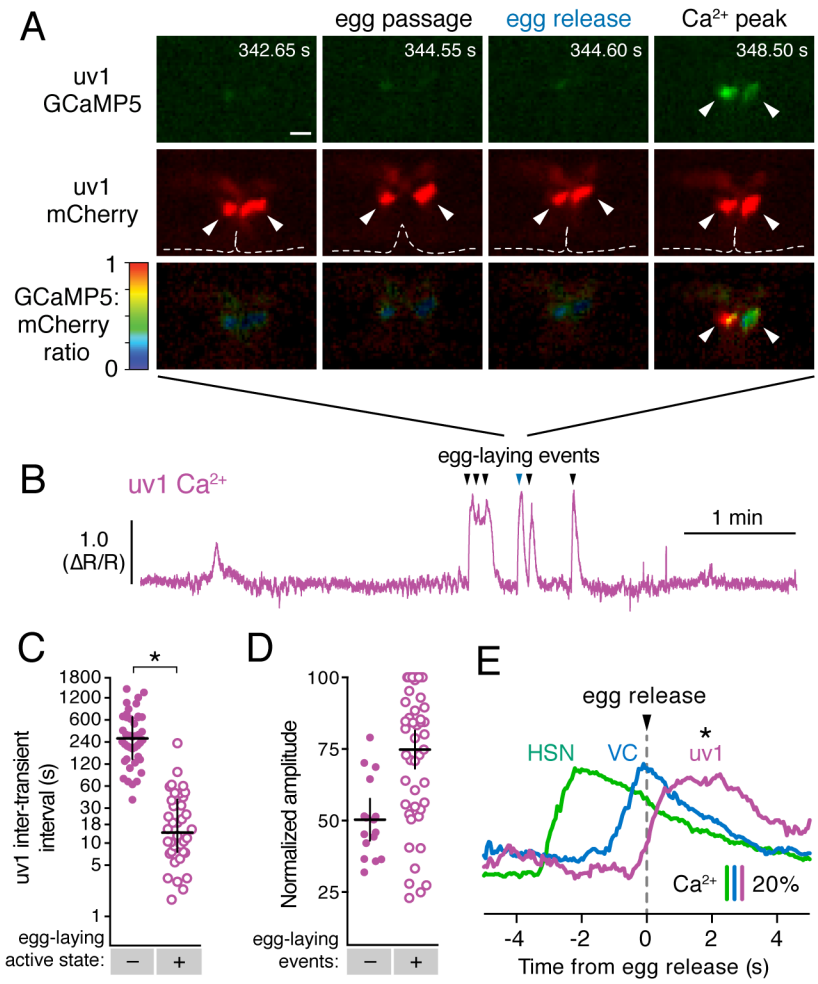

Figure 5. The tyraminergic uv1 neuroendocrine cells are mechanically deformed and activated by egg laying.

(**A**) Fluorescence micrographs of uv1 showing GCaMP5, mCherry, and the GCaMP5/mCherry ratio before egg laying, during egg passage through the vulva, and after egg release. Times of movie frames in seconds are at top, and white scale bar is 10 μm. Arrowheads in mCherry micrographs indicate position of uv1 cells as they are deformed by egg passage, the dotted line indicates position and opening of the vulva. (**B**) GCaMP5/mCherry ratio (ΔR/R) trace of uv1 activity, including an egg-laying active state. Egg-laying events are indicated by arrowheads. (**C**) Scatter plots of uv1 inter-transient intervals during the inactive (closed circles)

877 and active (open circles) egg-laying behavior states. Line indicates median, error bars indicate
878 quartiles, and asterisks indicate significant differences (p<0.0001). (**D**) Scatter plots and
879 medians of normalized amplitude with (+; open circles) and without (–; closed circles) an
880 accompanying egg release. Error bars indicate quartiles, and asterisks indicate significant
881 differences (p<0.0001, Mann-Whitney test). (**E**) uv1 Ca^{2+} transients follow egg-laying events.
882 Normalized traces of median Ca^{2+} in HSN (green) and VC (blue) from Figure 1 are compared
883 to uv1 (purple), synchronized to the moment of egg release (0 s, arrowhead and dotted line).
884 Bars indicates 20% change in median GCaMP/mCherry ratio. Asterisk indicates the uv1 Ca^{2+}
885 peak is significantly later than the HSN and VC peaks (p <0.0001; n=27 egg-laying events from
886 13 animals).

887

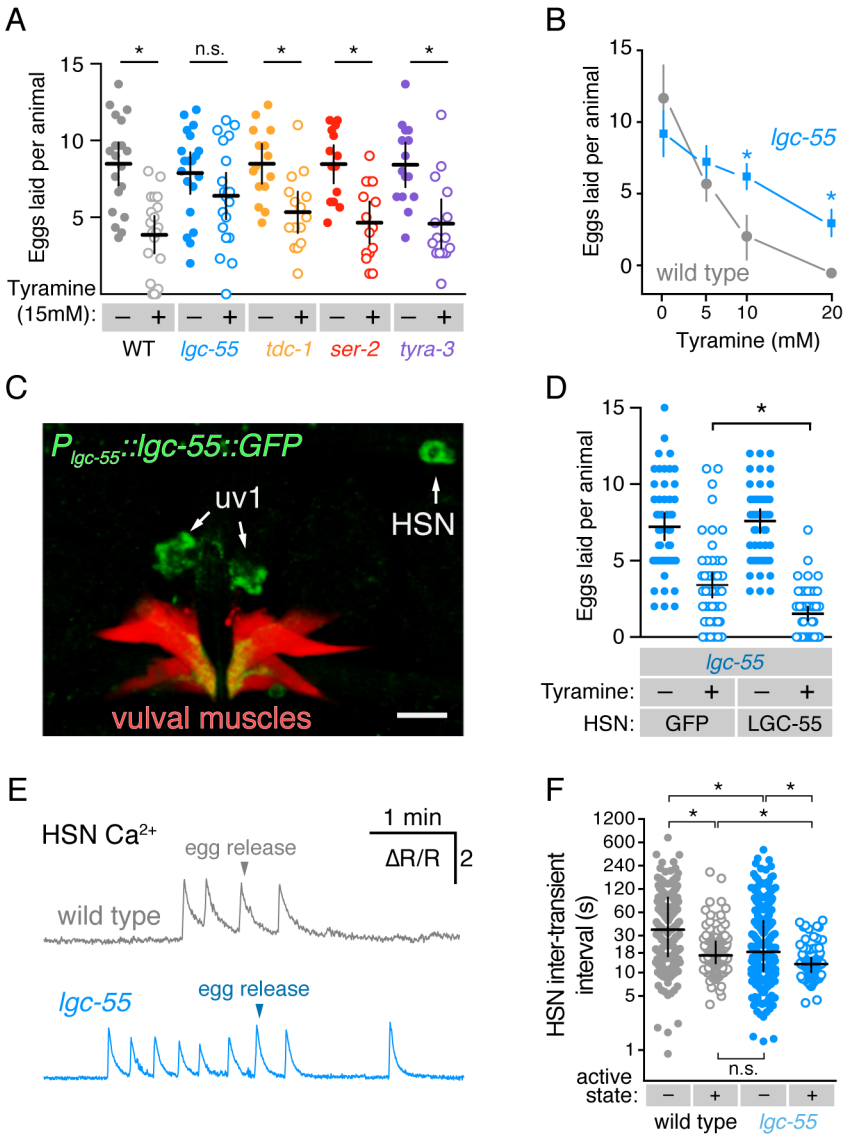

Figure 6. Tyramine inhibits egg laying, in part, through LGC-55 receptors on the HSNs.

(**A**) Exogenous tyramine inhibits egg-laying behavior and requires the LGC-55 receptor. Scatter plots and means showing the number of eggs laid after 30 minutes by wild type (grey), *tdc-1(n3419)* tyramine biosynthetic enzyme mutant (blue), and *lgc-55(tm2913), ser-2(pk1357)*, and *tyra-3(ok325)* tyramine receptor mutant animals (orange, red, and purple, respectively) on plates without (-, closed circles) or with (+, open circles) 15 mM tyramine. Error bars indicate 95% confidence intervals, and asterisks indicate significant responses (p<0.01) while n.s. is

896 not significant (p>0.05). (**B**) Dose-response curve of tyramine inhibition on egg laying in wild-
897 type and *lgc-55* mutant animals. Asterisks indicate significant differences at 10 mM (p<0.0001)
898 and 20 mM tyramine (p=0.0164). (**C**) LGC-55 is expressed in HSN, uv1, and vulval muscles.
899 Expression of LGC-55 tagged with GFP compared to vulval muscle mCherry was visualized
900 using confocal microscopy; scale bar is 10 μm. GFP is localized to the HSN and uv1 cell
901 bodies (arrows) as well as the ventral tips of the vulval muscles. (**D**) Re-expression of LGC-55
902 in HSN restores tyramine inhibition of egg laying. Scatter plots of eggs laid by *lgc-55* mutants
903 expressing either GFP or *lgc-55* in the HSN from the *tph-1* promoter. Asterisk indicates
904 significant differences in egg laying (p=0.0029). (**E**) Loss of LGC-55 increases HSN activity.
905 Representative Ca^{2+} ratio traces show HSN activity in wild type (top, grey) and *lgc-55* mutant
906 animals (bottom, blue) during the active state. (**F**) Scatter plots and medians of HSN inter-
907 transient intervals in wild type and *lgc-55* mutant animals during the egg-laying inactive (–,
908 closed circles) and active (+, open circles) states. Asterisks indicate statistically significant
909 differences (p<0.0001; n≥7 animals per genotype).

910

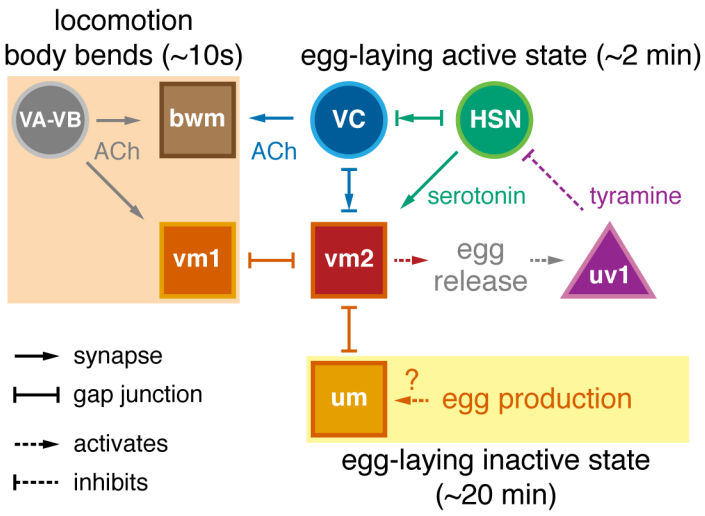

Figure 7. Working model of how circuit connectivity, signaling, and activity contribute to the observed rhythms that accompany the active and inactive egg-laying behavior states. VA and VB motor neuron synapses release acetylcholine (ACh) that rhythmically excites the body wall muscles (bwm) and vm1 vulval muscles during each locomotion body bend, every ~10 seconds. Eggs are produced from each gonad arm every 10 minutes, and we propose the accumulation of 2-3 eggs mechanically excites the uterine muscles (um) facilitating exit from the inactive state. Sustained bursts of HSN command motor neuron activity trigger serotonin release that drives ~2 minute active states. HSN also makes synapses and gap junctions with the cholinergic VC motor neurons, and VC makes synapses and gap junctions with the vm2 muscles whose contraction allows egg release. Passage of eggs mechanically activates the uv1 cells triggering release of tyramine and neuropeptides, which inhibit HSN activity to terminate the active state. See text for further details.

925 **Movie 1.** Ratio recording of HSN Ca^{2+} transients during the egg-laying active state. High Ca^{2+}
926 is indicated in red while low calcium is in blue. Large panel is an expanded view showing the
927 freely-moving animal that has been contrast enhanced to make the worm and its laid eggs
928 visible. Inset is cropped to a small area containing the HSN, and stabilized to remove
929 movement. Text labels indicate when Ca^{2+} transients and egg release occur.

930 **Movie 2.** Ratio recording of VC Ca^{2+} transients during the egg-laying active state. High Ca^{2+}
931 is indicated in red while low calcium is in blue. Contrast is enhanced to make the worm visible,
932 although the laid eggs are not easily visible. Text labels indicate when vulval muscle (vm)
933 twitches or egg-laying contractions occur, which result in small or large displacements of the
934 VC4 and VC5 cell bodies, respectively.

935 **Movie 3.** Ratio recording of vulval muscle Ca^{2+} transients during the egg-laying active state.
936 High Ca^{2+} is indicated in red while low calcium is in blue. Large panel is an expanded view
937 showing the freely-moving animal that has been contrast enhanced to make the worm and its
938 laid eggs visible. Inset is cropped to a small area containing the vulval muscles, and stabilized
939 to remove movement. Text labels indicate when Ca^{2+} transients and egg release occur.

940 **Movie 4.** Activation of the HSNs using Channelrhodopsin-2 induces the egg-laying active state.
941 Animals were recorded for a total of 90 seconds with continuous blue light stimulation
942 beginning at 30 s and ending at 60s, during which five eggs are laid. Recording is sped up 3-
943 fold.

944 **Movie 5.** Activation of the VCs using Channelrhodopsin-2 induces animal paralysis and
945 shortening of body length. Animals were recorded for a total of 90 seconds with continuous
946 blue light stimulation beginning at 30 s and ending at 60s. Recording is sped up 3-fold.

947 **Movie 6.** Ratio recording of uv1 Ca^{2+} transients during the egg-laying active state. High Ca^{2+}
948 is indicated in red while low calcium is in blue. Large panel is an expanded view showing the
949 freely-moving animal. Inset is cropped to a small area containing the uv1s, and stabilized to
950 remove movement. Microscope is focused to image the two uv1 cells on the right side of this
951 animal, while the two additional uv1 cells on the left side are out of focus and not visible. Text
952 labels indicate when egg releases occur, each of which is followed by a uv1 Ca^{2+} transient.